Drug Delivery and Translational Research (2018) 8:1139–1151
https://doi.org/10.1007/s13346-018-0553-1

ORIGINAL ARTICLE

Production and characterization of drug-loaded toroidal vortices from a novel ocular drug delivery device

Matthew J. Herpin[1] · Dominik Ebi[2] · Noel T. Clemens[2] · Hugh D. C. Smyth[1]

Published online: 2 July 2018

Abstract

For the last several decades, the predominant method for delivering medicine to the surface of the eye has been the standard multiuse eye dropper. While being the most popular, this method has significant limitations. Recently, an effort has been made to explore the use of a directed toroidal vortex or "smoke ring" aerosol delivery system that may help overcome these limitations and enable delivery of precise amounts of formulation and drug to the ocular surface. Promising preliminary in vitro studies indicated dosing control, but the physical characteristics of the toriodal aerosol device performance and impaction forces related to patient comfort have yet to be established. Here, we experimentally investigate the mechanics and dynamics of these ocular aerosol vortices, including translational and rotational velocities, spatial droplet size distributions, and relative impaction forces in order to optimize the device performance and evaluate potential for clinical use. Maximal droplet velocity at various actuation forces was determined, and they were found to be all less than 6 m/s even at the highest actuation forces. Moreover, plume impaction forces were determined across a range of conditions and were all less than about 4.5 μN. Collectively, these studies showed that the physical and mechanical properties of the emitted drug-loaded vortices would be suitable for ocular administration.

Keywords Ophthalmic aerosol delivery · Precision dosing · Toroidal vortex · Ocular drug delivery device · Drug-device combination products

Introduction

The increasing prevalence in the age-related disease is especially notable in ophthalmology. It is estimated that between 1 and 4% of all patients over 45 years of age will be diagnosed with glaucoma [1], and between 6 and 22% patients over the age of 70 years will be afflicted with age-related macular degeneration [2]. These ocular diseases are the two leading causes of blindness in the USA, which collectively major visual disorders cost $35.4 billion annually and are expected to further increase with an aging patient demographic [3].

Despite new ophthalmic drug candidates to treat glaucoma and retinal disease, large barriers to the effective delivery of these compounds to the target tissues still remain. This is largely due to the highly protected nature of the ocular/visual system and its crucial role in survival throughout the evolutionary process. Beyond the physical structures in the eye such as the cornea, sclera, iris, and cilliary body that can obstruct the diffusion of drugs from the front of the eye, there are also the blood-retina barrier and the blood-aqueous barrier. These barriers limit the entry of drugs from the bloodstream so that many systemically circulating medications do not achieve adequate concentrations in the ocular tissues [4]. The eye is also guarded with a reflex blinking and lacrimal flushing system from the anterior. This mechanism drastically reduces the available time for a drug to diffuse across the physical barriers of the front of the eye. Conventional ophthalmic drug delivery systems such as viscous solutions, suspensions, gels, and ointments attempt to increase the residence time and, thus,

✉ Matthew J. Herpin
matt.herpin@utexas.edu

Dominik Ebi
dominik.ebi@utexas.edu

Noel T. Clemens
clemens@mail.utexas.edu

Hugh D. C. Smyth
hugh.smyth@austin.utexas.edu

[1] Division of Molecular Pharmaceutics and Drug Delivery, College of Pharmacy, The University of Texas at Austin, 1 University Station, A1900, Austin, TX 78712-1200, USA

[2] Department of Aerospace Engineering and Engineering Mechanics, The University of Texas at Austin, Austin, TX 78759, USA

the exposure to improve absorption. However, due to the difficulties in administration and increased blurring of the vision, patient acceptability and compliance may become an issue. Other nonconventional dosage forms such as ocular inserts or drug-eluting punctal plugs have also been investigated and used for the purpose of decreasing dosing frequency and improving bioavailability [5]. While these have shown to be promising, they have limitations in that they can be inadvertently ejected from the eye which often requires a doctor's visit to reinstall the device. In addition, some patients complain of discomfort in wearing them, so at this point they have not yet been able to provide a complete solution.

Recently, pharmaceutical scientists have investigated the potential use of ophthalmic aerosols to deliver medications to the eye. In a clinical trial assessing mean maximal pupil dilations in 100 patients, Collins et al. found no significant difference between eye drops and an ophthalmic aerosol administered topically [6]. Moreover, others have previously shown improved drug bioavailability from smaller volume instillations [7–11]. In addition, the use of small volume instillations can significantly reduce the overall drug exposure to the patient and potentially eliminate or reduce some off-target effects, which is especially important in pediatrics [12–15].

Our laboratory has recently developed a method to deliver medications to the surface of the eye via aerosols which are formed into discrete doses utilizing toroidal vortices (e.g., "smoke rings") that enabled accurate and controllable delivery of small administered volumes [16]. Because this method of delivery is significantly different from other aerosol or small volume approaches tested previously, we investigated here several different analytical techniques for the characterization of this aerosol delivery system. This delivery technology produces micron-sized droplets containing dissolved drug, moving at variable velocities. Therefore, advanced analytical methods needed to be adopted to characterize this dynamic system, and these methods may prove to be useful in analyzing other aerosol systems such as nasal sprays and inhalation aerosols as well.

The objective of this study was to characterize the clinically relevant physical performance features of this delivery device, namely characterize droplet size dynamics during vortex delivery, the bulk vortex and individual droplet velocities, as well as the impaction force of the toroid onto a surface in order to determine if the device likely performs in a safe comfortable and reliable manner suitable for future clinical investigations.

Materials and methods

Materials

The Omron MicroAir NE22 vibrating mesh nebulizer was graciously donated by Omron Corp. EZ-Breathe Atomizer (Nephron Pharmaceuticals, Orlando, FL) was purchased OTC. All formulations utilized isotonic phosphate buffered saline, PBS (Sigma), or PBS and fluorescein sodium which was purchased from Spectrum Chemical MFG Corp., USA. The ocular toroidal vortex generator was custom fabricated in house.

Methods

Device actuation for the generation of toroidal vortices

Generating toroidal vortices from this ocular drug delivery device is based on two key major actions/steps: (1) the aerosol generation and (2) the ejection of the droplets. Aerosols were loaded into the chamber portion of the device via two different vibrating mesh aerosol generators, the Omron MicroAir NE-U22 and the EZ-Breath Atomizer. Once the chamber is adequately filled with the desired amount of aerosol, a 12-V push-pull type solenoid (Adafruit, USA) is activated in order to impart a force wave onto the actuating membrane. A variable voltage controller was used to alter the actuation energy supplied to the membrane actuator and thus alter the exit velocity of the toroidal vortices. This device actuation mechanism as well as the essential device components is illustrated in Fig. 1. The fundamental mechanism for vortex formation is the establishment of an area of low pressure at the edge of the orifice. As the pressure is built up inside the aerosol chamber, the internal fluid flow as well as entrained aerosol droplets is accelerated and is forced to pass the circular edge of the exiting orifice, and this forms a vortex that is congruent with the path of the orifice and allows the entrained aerosol to then be pulled into the circulating fluid flow.

Determination of the maximal droplet velocity within the toroidal vortex

Stereo particle image velocimetry High-speed stereoscopic particle image velocimetry (PIV) was utilized to measure the velocity field in a plane cutting through a propagating toroidal vortex with nebulized droplets entrained within. We generated a laser beam with a high-repetition rate Nd:YLF laser (Coherent Evolution 90) that was then formed into a thin sheet with bench top optics. This laser sheet was used to illuminate the droplets within the toroidal vortex at a frequency of 5 kHz to obtain a velocity field every 200 μs. This laser sheet is 25 mm wide and aligned with the device orifice (nozzle) to allow for tracking the velocity as it is generated to a distance of 25 mm. The spatial orientation can be seen in Fig. 2. Furthermore, the droplets were imaged with two high-speed Photron APX cameras equipped with Nikkor 105 mm lenses with an f/5.6 aperture. For the stereoscopic PIV setup, i.e., to capture the out-of-plane motion as well, the cameras were

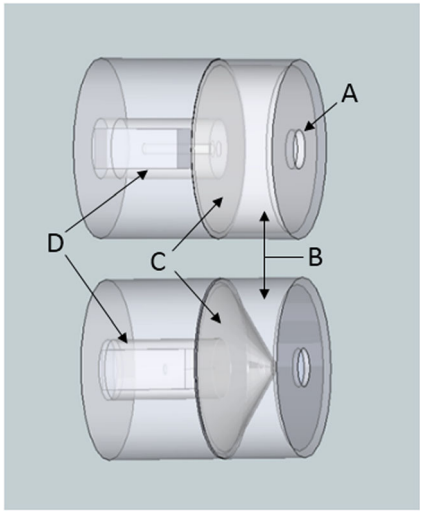

Fig. 1 Illustration of the actuation mechanism of the ocular delivery device. Above, at rest, and below while being actuated. Key device components—A: toroidal vortex forming exit orifice, B: aerosol chamber, C: actuation membrane, and D: electronic actuator solenoid

oriented at an angle relative to the light sheet normal vector as shown in Fig. 2.

The investigational space was calibrated with a dot-array target of known dimensions so that a mapping function between pixel location on camera and physical space could be established using the pinhole model. The cameras were synchronized with the laser to capture light scattered off of the droplets at 5 kHz at a resolution of 512 × 512 pixels. For PIV processing, the images were divided into 16 × 16-pixel interrogation windows with 50% overlap. The particle images in subsequent interrogation windows over time are cross-correlated to obtain the particle displacement. The velocity vector is obtained from the particle displacement and the time delay between two subsequent laser pulses (200 μs). We used the DaVis 8.2 Software package by LaVision to perform PIV processing at a spatial resolution of 0.055 mm/pix, which leads to a measured velocity vector every 0.45 mm allowing for well-resolved velocity fields throughout the internal dimensions of the vortex.

Toroidal vortex translational velocity

In order to determine the velocity at which the entire toroid propagates, a different approach was taken. The high-speed image sequences allow for temporally resolved measurement of the velocity by mapping them to physical space via the dot-array target calibration previously mentioned and employing Matlab in conjunction with its image processing toolbox. The velocity of the toroidal vortex is determined based on tracking the front edge of the toroid over time, which is comparable to what others have done using the "dark field technique" to characterize metered dose inhalers [17]. Except in this case, the front edge detection was automated and based on an intensity threshold. The velocity evolution was obtained by a sliding linear curve fit to the change in position over time.

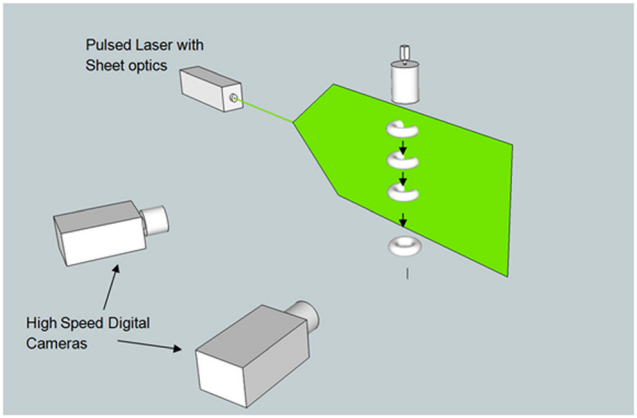

Fig. 2 Schematic of the experimental setup of stereoscopic particle image velocimetry

Droplet size analysis

The aerosols produced from this device were characterized for particle/droplet size distribution (PSD) and optical concentration (C_{opt}) by laser diffraction (Sympatec-Helos) using the Fraunhofer (HRLD) and Mie Theory calculation methods, and data was collected using an optical trigger. The PSD of the aerosol is characterized by the X_{10}, X_{50}, and X_{90} of the aerosol, and the terms in subscript refer to the percentage of droplets by mass that are below the diameter in micrometers by mass. The modular dispersing units were removed and the instrument was set up in the "open-bench" mode where the aerosol can be transmitted from the device directly into the beam path for analysis. The instrument was set to collect PSD/C_{opt} data at a 1-ms interval throughout the duration of the toroid propagation. A schematic on how the vortices were analyzed is illustrated in Fig. 3.

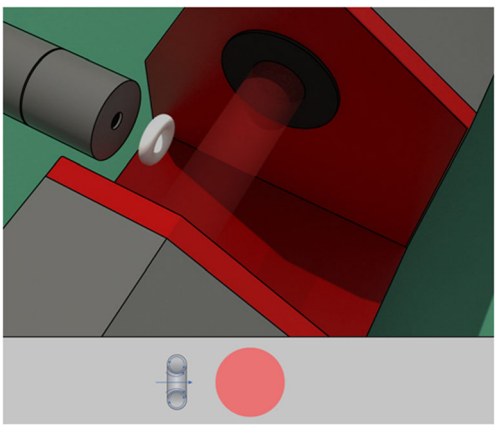

Fig. 3 Schematic showing the experimental setup for the droplet size analysis of a toroidal vortex by laser diffraction

Plume impaction force

In order to assess the relative impact force generated by these toroidal vortices, we custom configured a Mettler Toledo XP26 precision microbalance. The balance was connected via serial port to a computer with data-logging software. The balance was configured into fast-host mode and balance measurements were streamed at the maximal sampling rate of 97/s (Mettler Toledo manual). The device was placed inside the glass wind cage and an additional wind shielding apparatus/stand was built to add further protection from convective wind and to align the device. The device was actuated perpendicular to the balance plate at a distance of 3 cm in order to record direct deflections at a clinically relevant distance. Peak balance deflections were recorded and plotted vs. actuation energy to resolve the correlation relationship. See Fig. 4 for the experimental setup.

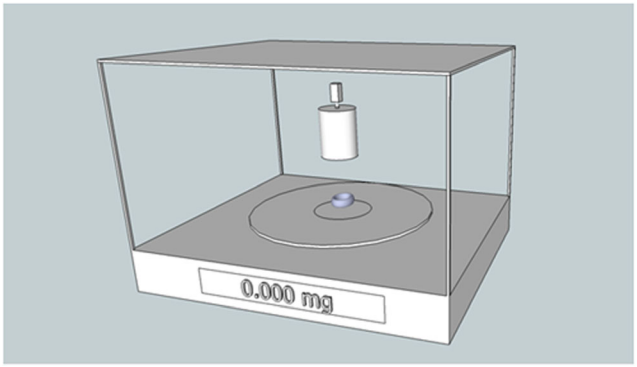

Fig. 4 Schematic for measuring the relative peak force generated by toroidal vortices

Results and discussion

When designing an ophthalmic drug delivery device, several key features need to be investigated in order to ensure patient safety, tolerability, reproducibility, feasibility, and ultimately, efficacy. The features of this device that have been identified to play a major role in the performance and feasibility of the device are related to the nature of the generated toroidal vortices and how a patient may experience them. The main features we investigate here are the components that can contribute to the patient comfort and usability. The components that contribute to the comfort of administration are all related to the nature of the impact of the droplets onto the eye and the velocity and size of droplets. In addition, these parameters also influence the performance because there exists a balance between velocity and PSD for optimal deposition because inertial deposition is governed by the mass and velocity of the individual droplets. Furthermore, the feasibility of the device pertains mostly in the ability to deliver the medicine before an instigated blink reflex can block or disrupt the dose [18]. For this, the bulk velocity over a distance was mapped to determine if the velocity of the vortex is adequate to escape a possible blink reflex.

We found that we were able to successfully characterize the major characteristics of these toroidal vortices utilizing different high-precision instrumentation/techniques such as laser diffraction, high-speed stereoscopic PIV, and microbalance real-time data sampling. Each of the methods discussed here help to determine the clinical feasibility of using this device in patients suffering from various ocular diseases. While these methods are currently being investigated for applications in ophthalmology, they could also be applied to investigate other aerosol or mist devices which create very small aerosol plumes. This paper is primarily concerned with investigating the properties of these toroidal vortices and the relevant aspects the patient would directly experience, in order to tune and optimize a final prototype device for further investigation in a clinical setting.

Droplet/particle size analysis and optical concentration

Droplet sizes within the vortex

It is expected that the physicochemical properties of the droplets generated from this device play a crucial role in the performance, because the droplet size can affect the deposition efficiency, dose payload, and even the net impact force onto the ocular surface. The mechanism by which these aerosols are produced (prior to formation of the vortex) is very similar to that of those produced for pulmonary inhalation (e.g., vibrating mesh nebulization), except that these droplets are first accumulated into a loading chamber and then emitted from the device and directed as a vortex onto the ocular surface. When generating nebulized aerosols for pulmonary inhalation, the patient would typically directly inhale the droplets as they are being generated. Because the droplets produced from these nebulizers are small (generally less than 10 μm), they are susceptible to the Kelvin effect, where the increased surface area causes an increase in the vapor pressure. This causes liquid within the droplet to evaporate quickly when below the vapor saturation point of the atmospheric phase [19]. As they enter the environment in the lungs, where the relative humidity is near 100%, the evaporation rates can be reduced, and in some cases, the droplets can even grow due to the nonvolatile solute concentration and hygroscopicity [20, 21]. In the case of the vortex delivery system with a loading chamber, droplets are generated and accumulated within the chamber prior to being emitted. Therefore, it was anticipated that there will be simultaneous evaporation/condensation as well as coalescence of the droplets within the chamber, and as they are emitted, there could be some evaporation. To determine the output of the device, we investigated droplet size and

optical concentration as a function of both chamber fill time and distance from the orifice. As a reference point, we selected an intermediate or a center point for the variables in consideration. A chamber fill time of 3 s, an actuation distance of 3 cm, and an actuation voltage of 9 V were selected. The characteristics of the toroids created under these conditions are shown in Table 1.

Droplet size and optical concentration as a function of chamber fill time

In order to generate drug-loaded toroidal vortices by this method, the aerosol chamber must first be temporarily filled with aerosol. This allows for a predetermined amount of aerosol to be incorporated in the vortices upon actuation. However, as previously mentioned, there is likely simultaneous droplet evaporation/condensation as well as coalescence. In order to assess the degree in which this may occur, we measured the optical concentration and droplet size characteristics for a fast and slow chamber fill time, corresponding to 1 and 3 s. The optical concentration can serve as in indicator of aerosol concentration or number of aerosol droplets per volume. The optical concentration can also serve as an indicator for the total amount of mass that is entrained in the gas phase. In addition, any change in droplet size would indicate if there was either evaporation or condensation occurring in the time frame in question. The results are reported in Table 2. The table shows that between a 1-s fill time and a 3-s fill time, there was practically no difference in X_{10} and X_{50} fraction and it was shown that there is a very small increase in X_{90}. However, there was a marked increase in optical concentration, from 3.01 to 11.95%. This increase was expected because the output rate of the nebulizer is constant, and by increasing the fill time, the number of droplets/volume increases proportionally. These findings are important because they show that despite increasing the number of droplets in the chamber, over the course of a 3-s period (which is likely a much longer period than will be used typically for a chamber fill), there is no appreciable evaporation or coalescence of droplets occurring in the chamber that translates to a measurable difference once the toroidal vortex is emitted from the device. This is an important characteristic because variability in droplet size distribution can ultimately increase the variability in the delivered dose available for absorption.

Vortex droplet size over distance

For practical purposes, it is not feasible to investigate the droplet sizes from within the device chamber, and the most important feature for deposition is the size of the droplets as they approach the ocular surface. So we investigated the effect of droplet size change as the vortex propagates from the orifice to a distance of 5 cm. This distance is considered practical limit for administration to the eye. As can be seen in Fig. 5, the X_{90} for the droplets decreases as the distance from the orifice increases. More specifically, at 1 cm from the orifice, the droplets have an X_{90} of ~4.25 μm, and as the distance increases to 3 cm, this value drops just slightly, but at 5 cm, the droplets are noticeably smaller with an X_{90} of ~3.25 μm. To further investigate, the optical concentration as a function of time was also assessed. We found that as the distance from the device orifice increased, the optical concentration also decreased (Fig. 6). Because the optical concentration is affected by both the number and size of the droplets in the beam path, as the droplets evaporate, they allow more light to pass through the aerosol and thus decrease the obscuration. These findings strongly suggest that there is some degree of evaporation occurring for these formulations as they propagate in a vortex, but the change is relatively small over the distance of interest. Furthermore, these results have provided insight that can serve as a guide to establish proper positioning of the device relative to the eye in order to minimize variability that could be caused by evaporation. Finally, the composition of the formulation will play a role in the effects of evaporation and droplet size generation. Previous studies have been conducted on the effects of hygroscopicity and how it relates to droplet growth and/or reduction due to evaporation [20]. Upon incorporation of different drug formulations, this will have to be taken into consideration to ensure that droplets remain in the desirable size range for the given application.

Table 1 Droplet size data for toroids generated from a 3-s fill, 9-V actuation at 3 cm distance (units for $X_{10,\ 50,\ 90}$ are in micrometers, and C_{opt} is in percentage)

Toroid sample no.	X_{10}	X_{50}	X_{90}	X_{opt}
Toroid 1	1.06	2.36	4.27	11.16
Toroid 2	0.90	2.34	4.60	10.56
Toroid 3	0.98	2.39	4.55	14.09
Average	0.98	2.36	4.47	11.94
Std	0.08	0.03	0.18	1.89

Table 2 Optical concentration and droplet size as a function of chamber fill time at a distance of 3 cm and 9 V actuation (units for $X_{10,\ 50,\ 90}$ are in micrometers, and C_{opt} is in percentage)

	1-sfill time				3-s fill time			
	C_{opt}	X_{10}	X_{50}	X_{90}	C_{opt}	X_{10}	X_{50}	X_{90}
	3.11	0.94	2.22	4.16	11.16	1.06	2.36	4.27
	1.91	0.83	2.07	4.09	10.56	0.90	2.34	4.60
	4.02	0.96	2.2	4.06	14.09	0.98	2.39	4.55
Average	3.01	0.91	2.16	4.10	11.94	0.98	2.36	4.47
Std	1.06	0.07	0.08	0.05	1.89	0.08	0.03	0.18

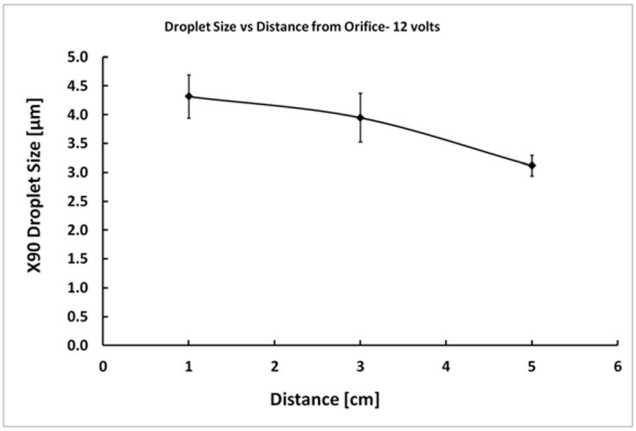

Fig. 5 Droplet size (X_{90}) decreases as the distance from the orifice increases

The typical droplets produced from vibrating mesh nebulizers range on the order of 1–5 μm, and this range can shift a few micrometers to the larger or smaller end with some formulation changes. However, for the most part, the droplets produced from these nebulizers are largely dependent on the nebulizer characteristics such as mesh size and energy amplitude [22]. As can be seen in Table 1, when the toroidal vortex was measured directly, the PSD falls roughly into this range. However, a slightly different strategy must be employed when measuring the PSD of droplets in a dynamically changing plume, and in our case, we are mostly concerned with the large droplets, which carry the majority of the payload of the medicine. For reference, a single 10-μm droplet can carry 1000 times more mass than a 1-μm droplet. Furthermore, it is known that upon forming a vortex, some droplets can be ejected from the core filament dependent upon their size and density and the viscosity of the gaseous media [23]. This could potentially cause a size segregation of the droplets spatially within the vortex and as the toroid propagates. Thus, it is important to note where the payload of the dose is located in relation to the vortex geometry because this could influence the amount of drug available for deposition onto the surface.

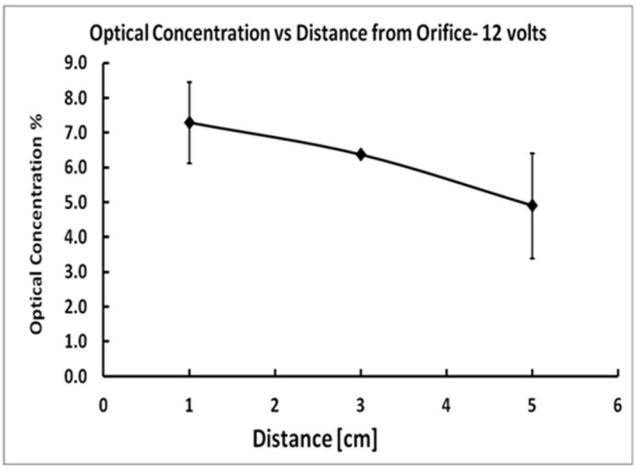

Fig. 6 Toroidal vortex optical concentration as a function of distance from the device

In order to assess the dynamic changes in droplet size within a toroidal vortex, we utilized laser diffraction with ultra high-speed time slicing (0.5 ms time base). This allows for the determination of the PSD of the droplets spatially within the toroidal vortex including (a) the leading edge of the vortex, (b) the center point when the toroid is completely within the beam, and (c) at the trailing edge of the vortex. These special cases are illustrated in the following figures, respectively: (a) Fig. 7, (b) Fig. 8, and (c) Fig. 9. Furthermore, the optical concentration was also measured simultaneously in order to assess the onset of the vortex entering the laser. A time-resolved plot of optical concentration (C_{opt}) and the X_{90} droplet size are plotted in Fig. 10 (labels A, B, and C correspond to regions of the toroid previously mentioned). Because the vortices are highly symmetrical, the leading edge of the vortex is representative of the outer edge or the shell of the toroid. In the laser diffraction data plot in Fig. 10, it can be seen that as the toroid moves through the beam path, there is a decrease in droplet size and as the toroid leaves the beam (i.e., the rear edge of the vortex), the droplet size increases again. More specifically, in this example, the leading edge of the toroid, labeled A, has an X_{90} of 5.75 μm, while in the center, it drops down to 5.15 μm, and then as it exits, the size increases to 6.58 μm. This differential in size could be due to the aforementioned effect where droplets can be segregated in vortical flows based on their size and the relative velocity of gas in which they are entrained. Furthermore, it appears that the larger droplets are ejected from the core due to inertia, and occupy the outer shell of the vortex, while the smaller droplets either remain in the core or drift inward due to the drop in relative pressure caused by the vortex. However, it should be mentioned that it is also possible that due to the increased number of droplets that are present when at the peak optical concentration, multiple light scattering events could be contributing to this observed change. Multiple light scattering cannot be ruled out completely, but it is unlikely as our measurements

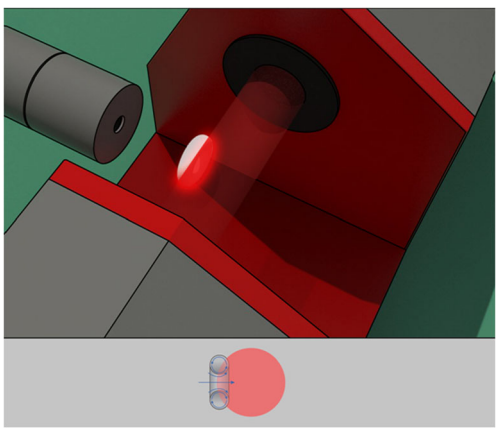

Fig. 7 Front edge of a toroidal vortex entering the laser diffraction beam

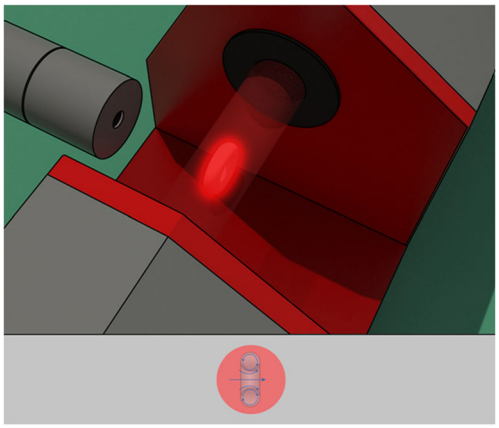

Fig. 8 Toroidal vortex is entirely inside laser diffraction beam

took place below the recommended limit for optical concentration of 15% outlined in USP<429>. Nonetheless, it can be seen directly that the PSD of the droplets is not changed to the scale that would affect their deposition and thus their performance for ophthalmic applications.

Another feature that is noticeable when looking at the optical concentration-time curve from Fig. 10, it can be seen that the signal does not return to the baseline. This is due to the lingering tail that exists during the early stage of vortex formation. These are droplets that are too large or too far away from the entrainable fluid flow to be captured into the vortex and thus form a streak as the vortex propagates. This streaking is also visible in the high-speed video frames (Fig. 11). Finally, from the data point at label C, it can also be seen that the size of the droplets in the tail is larger than that in the core and more comparable to that of the front edge of the vortex, further supporting the notion that the radially centered portion of the vortex does in fact contain the smaller droplets [23].

Toroidal vortex propagation dynamics

Another critical aspect of the device is the ability to deliver the aerosol at an effective, safe, and comfortable speed. A high-

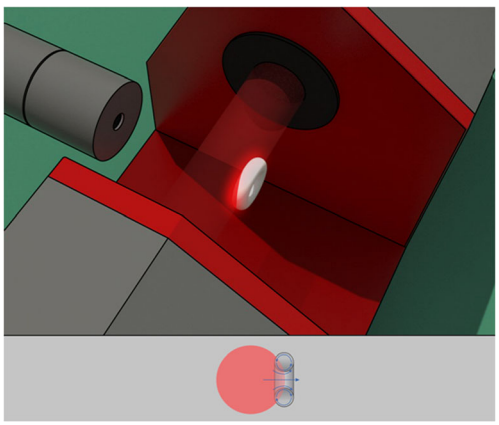

Fig. 9 Back edge of a toroidal vortex illuminated by the laser diffraction beam as it exits the beam path

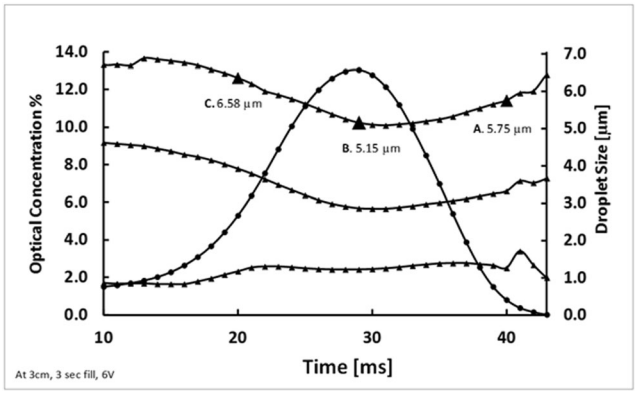

Fig. 10 Optical concentration plotted (solid circles) and droplet size X_{90} (μm) (solid triangles) plotted as a function of time. Label A indicates the front edge of the toroidal vortex. B When the toroid is entirely in the laser beam path. C The back/outside edge of the toroid

level balance between droplet velocity and impaction force is required here, because the aerosol needs to be moving fast enough to impart adequate inertial characteristics onto the droplets so they can be deposited effectively on the eye surface without being intercepted by a possible blink reflex, while still being gentle enough to not cause discomfort.

The propagation of the toroidal vortex can be broken into two main components: (1) the bulk velocity of the vortex ring as whole (translational) and (2) the net or max droplet velocity within the vortex (rotational velocity plus translational). The bulk velocity of the plume was measured by tracking the front edge of the toroid; this provides information as to how long it will take for the vortex to reach the eye at a set distance. In addition, because the vortex velocity was tracked at a distance, we can determine the optimal spacing from the nozzle and account for any deceleration if the eyepiece spacer needs to be adjusted.

Previous studies had shown that the velocity of an emitted vortex was proportional to the actuation force; however, that velocity data was produced using a calibrated pendulum which is not feasible for patient use [24]. An electronic actuator was built to impart the forces required to generate the toroidal vortices, and the control was modulated with a variable voltage supply. The device was then actuated at a low, medium, and max voltage to obtain a velocity profile for each actuation energy level as well as for each device over the distance relevant for delivery to the eye (~3 cm). The bulk velocity associated with the EZ device is displayed in Fig. 12, and the OMR device bulk velocity is shown in Fig. 13. The shaded areas indicate the uncertainty (standard deviation from five runs) associated with measured bulk velocities. The results show that the bulk velocities are quite reproducible and only slightly decrease over the distances measured. Furthermore, it can be clearly seen that there is a noticeable difference in the bulk velocity of toroids for each level of

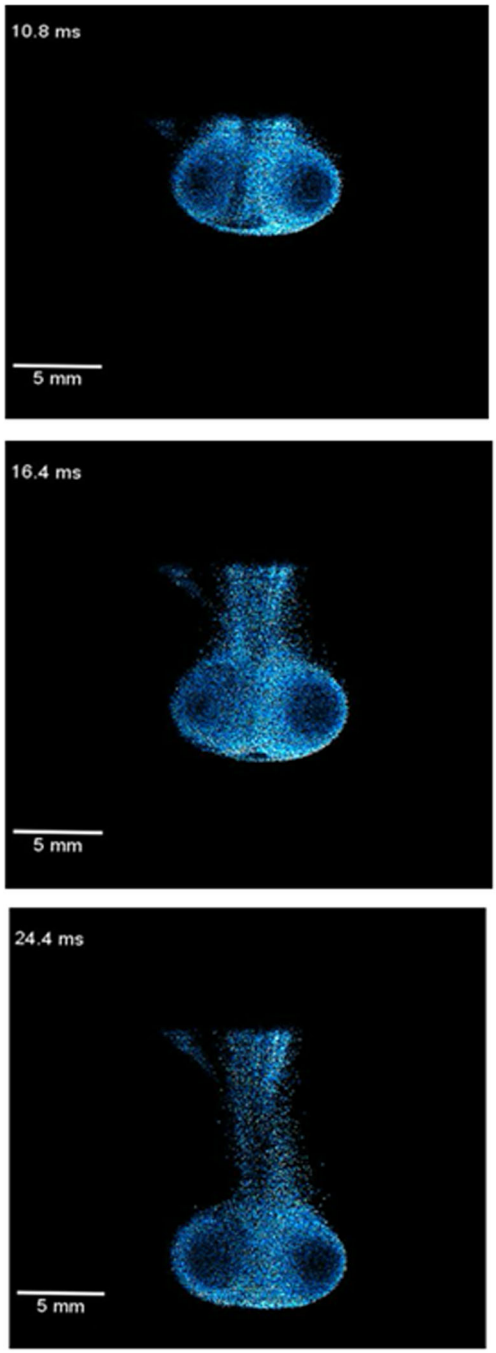

Fig. 11 Cross-sectional view of a toroidal vortex propagating at 5000 frames per second

actuation energy and also between devices. The EZ device has a nearly double bulk velocity at each actuation energy than that of the OMR device. We attribute this difference in velocity to the nature of the venting on the aerosol generator. Because the chamber is relatively sealed when force is applied to the actuating membrane, the pressure inside the chamber is momentarily built up. In the case of the OMR device, designed venting from within the device allows for this pressure buildup to dissipate more readily, therefore reducing the

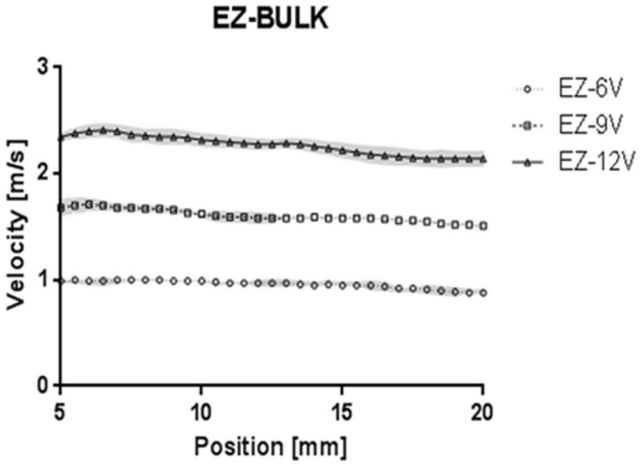

Fig. 12 Bulk velocity of toroids generated from the EZ-atomizer equipped device, as a function of distance from the device orifice

amount of energy that is directed toward ejecting the toroidal vortex. Nonetheless, despite the geometric differences and internal venting dissimilarities in the aerosol generators, each of the devices produced very reproducible velocity profiles. Furthermore, for each of the devices, the velocities only dropped by approximately 10% from the nozzle to a distance of about 25 mm, where they would likely impact eye. This will be useful information for determining the optimal distance to set the orifice relative to the eye for administration.

Overall, we found that in all of the cases, even the slowest moving toroid from the slowest device (OMR at 6 V), the amount of time it would take to deposit is on the order of 30 ms from actuation to contact. This is clinically relevant because the amount of time it takes for the human blink reflex is nearly 300 ms. This means that even if the actuation of the device causes a reflex blink, the toroid would have already exited the device and impacted the eye before the eyelid could close and block the dose. However, these findings do not rule out the possibility of the patient having an anticipatory blink or "normal blink" which starts from before the device is actuated.

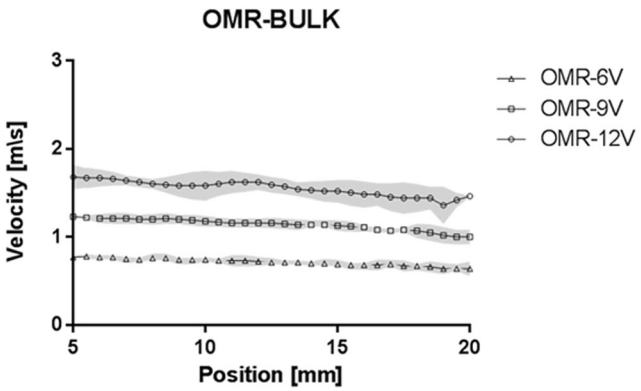

Fig. 13 Bulk velocity of toroids generated from the Omron equipped device, as a function of distance from the device orifice

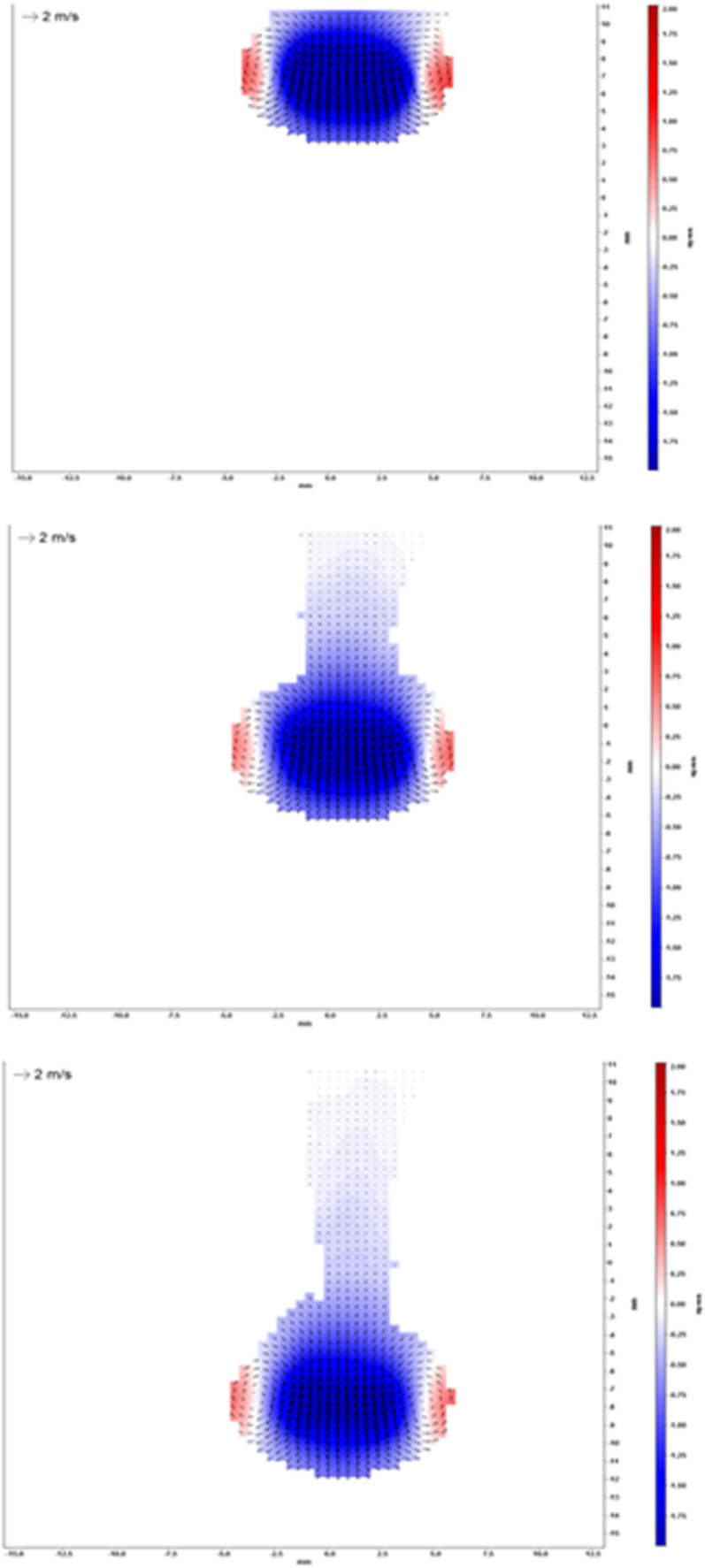

Fig. 14 Stereoscopic particle image velocimetry-2D contour plots for droplet velocity vectors

Beyond testing the bulk velocity of the toroids, it is also important to determine the maximal velocity of the droplets within the toroidal vortex because the droplets are circulated. This takes into account the bulk velocity plus the rotational velocity. This velocity has major implications in terms of assessing inertial deposition and net impact force onto the eye. As can be visualized in the 2D velocity contour plots in Fig. 14, the internal core of the vortex is where the maximal velocity is located. This is because as the vortex propagates, droplets within the vortex are rotating around an axis to the left and to the right of the vortex center plane, respectively. It is important to note that the center of the bulk flow shown in Fig. 14 is calculated by averaging 16 × 16-pixel interrogation windows with 50% overlap. This causes a blending or averaging of the velocities with their adjacent droplets and makes the 2D contour plot appear to have a measurable velocity in the core when there are no droplets present. There are essentially two rotating halves: one clockwise and one counterclockwise. This rotating motion of the droplets thus increases the total velocity (bulk velocity of vortex plus relative velocity of droplets) of those droplets that are in the core of the vortex at any point in time (indicated by the blue region of the 2D velocity contour plot). The opposite is the case in the outer regions of the toroid, where the droplets are actually moving in the opposite direction relative to the toroid propagation (indicated by the red region on the 2D velocity contour plot). Furthermore, at the front and rear edge of the vortex, the droplets would be moving perpendicular to the bulk velocity as the vortex rotates. This contrasting velocity field has an interesting effect on the performance, because at low bulk velocity (translational) speeds, the rotational velocity is high enough to cause a net negative velocity in the outer regions of the vortex seen in the contour plot in Fig. 14. This is important because these droplets will not be available for deposition onto the surface because they will not have forward inertia and they can be effectively subtracted from the available surface area of impaction. However, this net negative effect on the outer edges is eliminated at higher toroid velocities, thus increasing the effective impact surface area. In this case, the total forward moving velocity overcomes the rotational velocity, and thus, the entire toroidal surface area then becomes available for deposition, which can help to explain the observed higher dose deposition which occurred at higher speeds that was reported previously [24].

In summary, each of the devices tested showed a high level of precision and reproducibly when generating aerosol plumes over a range of velocities. Moreover, the EZ device (Fig. 15) and the OMR device (Fig. 16) exhibited a nearly linear increase in bulk toroid and maximum droplet velocities across all of the actuation energies. This level of consistency and predictability will offer a higher degree of control when applying aerosol to the surface of the eye.

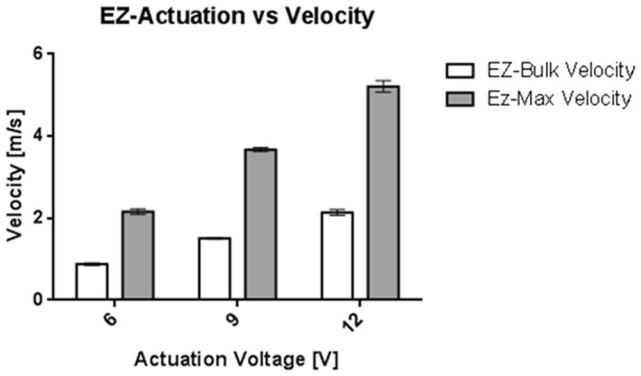

Fig. 15 Comparison between toroid velocity maximal drop velocity at different actuation energies for the EZ-atomizer device

Special considerations regarding uncertainty and assumptions

During the course of making PIV measurements and collecting data, uncertainty can arise in two main ways with PIV measurements. The first uncertainty pertains to the velocity magnitudes, and it is estimated that based on the correlation statistics approach that for all cases, it is found to be less than 0.04 and 0.1 m/s for the in-plane and out-of-plane motion velocity components [25]. The second aspect of uncertainty relates to the position of the laser sheet relative to the toroidal vortex. Because the goal of the experiment is to measure the velocity in a centerline cut plane in which the vortex travels, it is imperative that the orifice is properly aligned. However, a misalignment may still exist either from the onset or via drift as the vortex propagates. In order to correctly interpret the measured velocities, the stereoscopic PIV was employed. The alignment of the cameras is able to detect and obtain data from the out-of-plane velocity field.

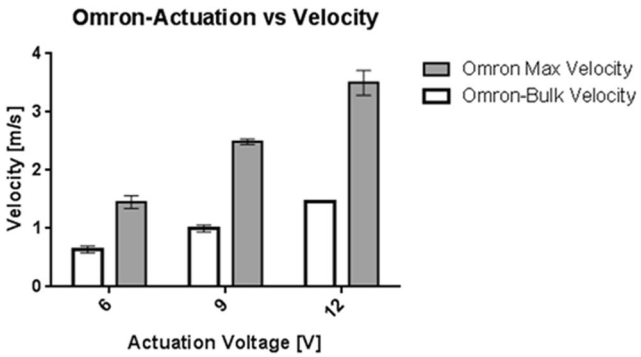

Fig. 16 Comparison between toroid velocity maximal drop velocity at different actuation energies for the OMR device

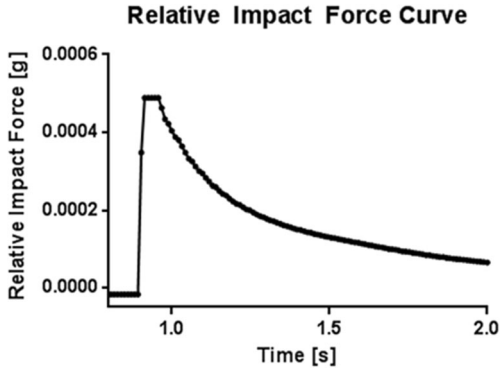

Fig. 17 Typical peak relative-force curve

Differences in aerosol-generating devices

In these experiments, we used two different aerosol-generating devices and attached them to the vortex drug delivery device. Both of the aerosol generators operate via the same aerosol production mechanism (i.e., vibrating mesh technology), but they have different specifications. Because they typically produce aerosols with similar size characteristics, any small differences in droplet size between the devices would not likely have an effect on the velocity data.

Relative impaction force

During the toroidal vortex velocity and PSD testing, we concluded that the EZ-Breathe-AG equipped device provided the widest range of velocities as well as an adequate PSD for evaluation in the relative impact force screening. This method was developed in-house to provide only in a relative sense the forces these toroidal vortices may impart onto a surface. Delving into the complexities of the impaction onto an actual ocular surface is beyond the scope of this manuscript. However, this analysis can provide guidance into evaluating the nature of the impaction and help to reduce concerns one may have about the comfort of the administration.

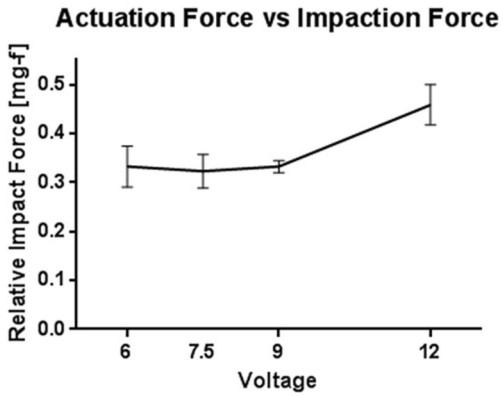

Fig. 18 Actuation force vs. relative impact force

When deciding which device and loading scheme to evaluate for this method, we had to consider the very small magnitude of the forces we were attempting to measure. Initial testing of the device without loading aerosol was found to be below the limit of detection of the microbalance. Previously, Guo et al. investigated impaction forces generated from nasal sprays and pressurized metered dose inhalers using a TA Instruments texture analyzer, which was turned onto its side and the doses were impacted onto the probe detector [26]. However, the forces in consideration in this study were found to be much lower in magnitude than this instrument would allow. Furthermore, Müller et al. investigated the impaction force generated by ophthalmic sprays using a piezoelectric transducer at several distances. In addition, Müller et al. have also developed techniques for measuring impaction force, but still none of these methods are sensitive enough to detect on the micro-Newton scale (< 1 mg-F) [26–28].

The principles of force measurement between our experimental setup and others are nearly identical. However, the piezoelectric transducer within the analytical microbalance is much more sensitive and allowed data to be streamed so that a peak force could be obtained. Upon actuating the device at a distance of 3 cm at low voltage, only a small deflection in baseline force was measured, on the order of about 0.3 mg. This was determined to be about as low as our balance would allow reproducibly. As the actuation voltage was increased, the impact force was only slightly altered, until the maximal actuation force of 12 V relayed a deflection of 0.5 mg, which correlates to about 4.5 μN. The microbalance was capable of reproducibly measuring these force curves, and a typical force-time curve is reported in Fig. 17. Figure 18 shows the relationship between actuation force and impact force. It was demonstrated that even at the highest actuation energy, there was only a very small increase in relative impact force.

Previously, Müller et al. showed that when comparing an eye drop to an eye spray, there was an inverse relationship between the distance of application and the force for the spray and a direct relationship between impact force for drops and distance. In essence, the drops gain momentum and impact harder the further they are away, while the spray loses velocity the further away it is administered. While this decrease in impact force from a distance is preferable, a drawback with spray type devices is that they emit aerosol in a cone-type geometry, meaning that the farther the device, the larger the diameter of the cone. Müller et al. found that at just a distance of 1 cm, the diameter of the cone was ~ 25 mm, and not only is this larger than the diameter of the exposed portion of the eye, this distance corresponds to an impact force of about 10 mN. This impact force corresponds to about a 1-g-force, nearly 2000 times the forces generated from the toroids found in our studies and triple the force created by an eye drop at the same distance. At an equivocal distance of 3 cm, the spray force from a spray is reduced ~ 5 mN, but at the cost of

increasing the diameter of the spray cone to about 35 mm, where a large portion of the spray is likely to miss the ocular surface. Furthermore, because the velocity and impaction forces of these toroidal vortices are so low relative to sprays or even eye drops, it very unlikely that there will be any disruption of the corneal surface or cause any discomfort for a patient.

Uncertainty in these measurements exists in the orientation of the device in that if the toroidal vortex does not directly impact the plate the results will be slightly different. In addition, if the vortex hits the center of the pan, this will cause a competing torque force on the lever arm. These results will be untrue to the method. Nonetheless, for the purpose of demonstrating the relative scale (semiquantitative analysis) of the impaction forces as they pertain to the clinical relevance of this device, this method was demonstrated to be satisfactory.

Conclusions

In summary, we found that despite the large differences in both bulk and maximal droplet velocity, the resulting impact forces generated from these toroidal vortices change very little, which is likely due to the small mass contained in each vortex. Furthermore, it was determined that this impact force is far below the threshold for what a patient could tolerate relative to other forces currently used clinically in patients. In addition, we also measured the size of the droplets to be on the order of which would be suitable and comfortable for ocular drug delivery and that the delivery of the toroid would likely outpace reflex blinking if it were to be triggered by the device. These preliminary studies have offered support for advancing the investigation into a preclinical setting and much more testing would need to be conducted to show the performance, safety, and efficacy of the delivery device in animal and human subjects.

Acknowledgments The authors would like to specially thank Dwight Mason for his technical assistance in graphics/illustrations.

Funding information The authors would like to kindly acknowledge the financial support from the PhRMA Foundation under the awarded Pre-Doctoral Fellowship in Pharmaceutics for Matthew Herpin.

Compliance with ethical standards

Conflict of interest The authors declare that they have no conflict of interest.

References

1. Weinreb RN, Khaw PT. Primary open-angle glaucoma. Lancet. 2004;363(9422):1711–20.
2. Zhang K, Zhang L, Weinreb RN. Ophthalmic drug discovery: novel targets and mechanisms for retinal diseases and glaucoma. Nat Rev Drug Discov. 2012;11(7):541–59.
3. Rein DB, Zhang P, Wirth KE, Lee PP, Hoerger TJ, McCall N, et al. The economic burden of major adult visual disorders in the United States. Arch Ophthalmol. 2006;124(12):1754–60.
4. Urtti A. Challenges and obstacles of ocular pharmacokinetics and drug delivery. Adv Drug Deliv Rev. 2006;58(11):1131–5. https://doi.org/10.1016/j.addr.2006.07.027.
5. Molokhia SA, Thomas SC, Garff KJ, Mandell KJ, Wirostko BM. Anterior eye segment drug delivery systems: current treatments and future challenges. J Ocul Pharmacol Ther. 2013;29(2):92–105.
6. Collins JF, Dartt DA, Dana R. Mist delivery of eye medication to the anterior segment. Am J Ophthalmol. 2007;144(1):137–9.
7. Halberg GP, Kelly S, Morrone M. Drug delivery systems for topical ophthalmic medication. Ann Ophthalmol. 1975;7(9):1199–204. 207-9
8. Martini LG, Embleton JK, Malcolmson RJ, Wilson CG. The use of small volume ocular sprays to improve the bioavailability of topically applied ophthalmic drugs. Eur J Pharm Biopharm. 1997;44(2):121–6.
9. Kahn M. Bioavailability of vitamin B12 using a small-volume nebulizer ophthalmic drug delivery system. Clin Exp Ophthalmol. 2005;33(4):402–7.
10. Diestelhorst M, Hellmich M, Hochrainer D, Roessler G, Steinfeld A, Zierenberg B. The ocular bioavailability from a new microspray MO. A comparison with conventional eye drops. Invest Ophthalmol Vis Sci. 2006;47(13):457.
11. Chrai SS, Patton TF, Mehta A, Robinson JR. Lacrimal and instilled fluid dynamics in rabbit eyes. J Pharm Sci. 1973;62(7):1112–21.
12. Elibol O, Alcelik T, Yuksel N, Caglar Y. The influence of drop size of cyclopentolate, phenylephrine and tropicamide on pupil dilatation and systemic side effects in infants. Acta Ophthalmol Scand. 1997;75(2):178–80.
13. Coulter RA. Pediatric use of topical ophthalmic drugs. Optometry. 2004;75(7):419–29.
14. Wheatcroft S, Sharma A, McAllister J. Reduction in mydriatic drop size in premature infants. Br J Ophthalmol. 1993;77(6):364–5.
15. Patton T, Robinson J. Pediatric dosing considerations in ophthalmology. J Pediatr Ophthalmol. 1976;13(3):171–8.
16. Smyth HD, Herpin MJ, inventors; Board of Regents, The University of Texas System (Austin, TX, US), assignee. Toroidal pharmaceutical formulations. United States patent # 9,119,773. 2015.
17. Hochrainer D, Hölz H, Kreher C, Scaffidi L, Spallek M, Wachtel H. Comparison of the aerosol velocity and spray duration of Respimat® Soft Mist™ inhaler and pressurized metered dose inhalers. J Aerosol Med. 2005;18(3):273–82.
18. Millodot M. Objective measurement of corneal sensitivity. Acta Ophthalmol. 1973;51(3):325–34. https://doi.org/10.1111/j.1755-3768.1973.tb06010.x.
19. Wiedensohler A, Stratmann F. Environmental particles. In: Gehr P, Heyder J, editors. Particle-lung interactions. New York: CRC; 2000. p. 75.
20. Hickey AJ, Martonen TB. Behavior of hygroscopic pharmaceutical aerosols and the influence of hydrophobic additives. Pharm Res. 1993;10(1):1–7.
21. Gehr P, Heyder J. Particle-lung interactions. New York: CRC; 2000.
22. Zhang G, David A, Wiedmann TS. Performance of the vibrating membrane aerosol generation device: Aeroneb Micropump Nebulizer™. J Aerosol Med. 2007;20(4):408–16.
23. Hasinger SH. Limit of centrifugal separation in a free vortex. AIAA J. 1971;9(4):644–8. https://doi.org/10.2514/3.6242.
24. Herpin MJ, Smyth HD. Precision ocular drug delivery via aerosol ring vortices. Pharm Res. 2017;34(11):2287–94.

25. Wieneke B. PIV uncertainty quantification from correlation statistics. Meas Sci Technol. 2015;26(7):074002.
26. Guo C, Ye W, Kauffman J, Doub WH. Evaluation of impaction force of nasal sprays and metered-dose inhalers using the Texture Analyser. J Pharm Sci. 2009;98(8):2799–806. https://doi.org/10.1002/jps.21648.
27. Müller F, Wagner M, Neubert R. Characterization of the force effect of aqueous and oily eye drops. J Pharm Sci. 2005;60(4):283–7.
28. Müller F, Wagner M, Neubert R. Comparative in vitro investigation of the forces exerted by eye drops and eye spray. J Pharm Sci. 2005;60(8):630–1.